engineering proceedings

MDPI

Proceeding Paper

Performance Analysis of a Commercial Aircraft Liquid Hydrogen Storage System †

Alireza Ebrahimi *, Andrew Rolt, Drewan Sanders and B. Deneys J. Schreiner

Centre for Aeronautics, Propulsion and Power, Cranfield University, Cranfield MK43 0AL, UK; a.rolt@cranfield.ac.uk (A.R.); d.s.sanders@cranfield.ac.uk (D.S.); b.deneys.j.schreiner@cranfield.ac.uk (B.D.J.S.)

* Correspondence: alireza.ebrahimi@cranfield.ac.uk

† Presented at the 15th EASN International Conference, Madrid, Spain, 14–17 October 2025.

Abstract

Liquid hydrogen (LH_2) fuel system architectures for aviation remain at low Technology Readiness Levels (TRLs) due to limited experimental data and the challenges of modelling cryogenic hydrogen's behavior. This paper presents a computationally efficient framework for sensitivity analysis that integrates cryogenic thermodynamics, tank geometry, external heat ingress, engine mass flow demands, and pressurization control strategies. A set of operational scenarios was modeled to demonstrate how tank pressure and temperature evolve under various control and geometric conditions, delivering five key insights: (1) Passive tank self-pressurization leads to continuous pressure rise and subcooled liquid. (2) LH_2 withdrawal alone may not fully stop pressurization with high heat ingress. (3) Gaseous hydrogen (GH_2) injection stabilizes pressure only up to moderate heat ingress during LH_2 extraction. (4) The addition of venting enables full pressure control. (5) Tank geometry and heat flux govern transient behavior. Spherical tanks show slower pressure and temperature rise than cylindrical ones, and both geometries maintain near-constant pressure at low heat flux. These insights offer practical guidance for designing reliable and thermally stable LH_2 storage systems for future aircraft applications, paving the way towards sustainable and zero-emission aviation.

Keywords: liquid hydrogen; LH_2; fuel system; aircraft; cryogenic tank; storage system

1. Introduction

Hydrogen (H_2) has emerged as the most viable and transformative solution for achieving a fully decarbonized aviation future, offering a pathway to eliminate in-flight CO_2 emissions entirely while significantly reducing other emissions [1]. It can be utilized in aviation via two primary pathways. For short-range to medium-range operations, hydrogen can be used via fuel cell technology, with water as the only byproduct, thereby eliminating both CO_2 and NOx emissions. For longer-range applications, where power density requirements are higher, hydrogen can be burned in redesigned gas turbine engines, maintaining compatibility with existing turbomachinery architectures while delivering zero CO_2 emissions [2,3]. Hydrogen has a gravimetric energy density of about 120 MJ/kg, nearly three times that of conventional jet fuel. This means that hydrogen-fueled aircraft only need one-third of the fuel mass to complete equivalent missions. Furthermore, hydrogen has a wide flammability range and rapid flame propagation, facilitating stable and efficient combustion under lean conditions. However, its adoption in aviation is not without technical challenges. The volumetric energy density of liquid hydrogen is roughly

Check for updates

Academic Editors: Spiros Pantelakis, Andreas Strohmayer and Gustavo Alonso

Published: 16 April 2026

Copyright: © 2026 by the authors. Licensee MDPI, Basel, Switzerland. This article is an open access article distributed under the terms and conditions of the Creative Commons Attribution (CC BY) license.

one-quarter that of conventional jet fuel. This requires much larger fuel storage tanks, which are typically cylindrical or spherical pressure vessels integrated into the aircraft fuselage, rather than being integral with the wings. Additionally, liquid hydrogen (LH_2) must be stored cryogenically at temperatures around 20 K, demanding advanced insulation systems and sophisticated thermal management to minimize boil-off losses and ensure operational safety [4]. These engineering complexities have been the focus of short-term studies, such as the UK ATI's FlyZero project [5] (completed in 2022) and Airbus' ZEROe program [6]. Airbus is now concentrating on hydrogen fuel-cell concepts together with MTU Aero Engines. Airbus's recent announcements indicate that their projected service entry timelines have changed by at least one new aircraft development cycle, underscoring the scale of the challenges associated with introducing LH_2 as a widely available aviation fuel.

The integration of cryogenic LH_2 storage systems into aircraft architectures represents one of the most critical technological barriers to hydrogen aviation. Unlike conventional jet fuel tanks, LH_2 tanks must simultaneously address multiple design requirements, including maintaining cryogenic conditions, managing boil-off losses, and minimizing weight. The complexity of these requirements has significant effects on overall system performance, aircraft range, and operational feasibility [7–10]. Although there has been a lot of research focused on specific elements of LH_2 tank design, for instance, optimizing the structure, assessing insulation effectiveness, and predicting boil-off losses, there remains a significant gap in comprehensive, integrated sensitivity analyses that systematically evaluate the coupled effects of multiple design parameters on overall tank system performance in aircraft applications [7,11]. Recent work by Burschyk et al. [10] applied global sensitivity analysis to LH_2 storage parameters for overall aircraft design. It identified gravimetric efficiency as a key output metric. However, their analysis focused on higher-level system integration rather than detailed tank-level thermodynamic behavior, pressurization control dynamics, and the operational trade-offs between different control strategies. Similarly, Adler et al. [11] developed a rapid zero-dimensional (0D) model for boil-off prediction, enabling optimization. However, they did not conduct a comprehensive sensitivity analysis across the full design parameter space, including geometry, thermal conditions, LH_2 extraction mass flow rates, and control strategies.

This research addresses the lack of a systematic sensitivity analysis framework that combines cryogenic thermodynamics, tank geometry, heat transfer, engine mass flow needs, and pressurization control strategies. Such a framework aims to identify the key design parameters and their interactions specific to aircraft LH_2 storage systems. The low-pressure (airframe) fuel system section analyzed in this study is illustrated in Figure 1, with a focus on the storage tank that is not sealed to investigate the effect of heat ingress to both the liquid and gaseous phases.

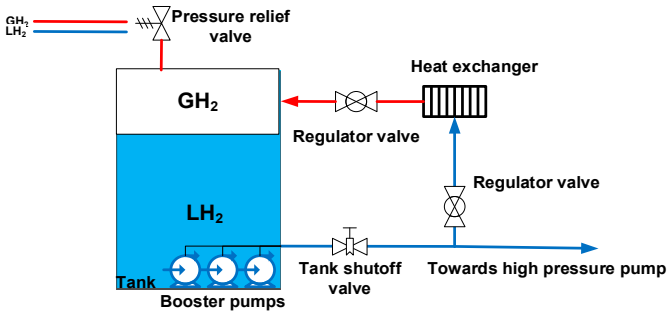


Figure 1. Simple schematic of a low-pressure (airframe) LH_2 fuel system.

2. Modelling of a Cryogenic Tank and Simulation Scenarios

2.1. Cryogenic Tank Modelling and Validation Setup

In this study, Siemens Amesim [12] software (version 2025) was used for modelling and simulation of the cryogenic tank systems, and the simulations were built on a similar approach provided in [13]. In the 0D lumped thermodynamic modeling of the tank, four equations were implemented: conservation of mass and energy, with one set applied to the liquid phase and another set applied to the gaseous phase. The model captures critical physical processes relevant to cryogenic aircraft fuel storage, including heat ingress from the external environment, pressurization behavior, and fuel withdrawal effects. The detailed mathematical formulation and governing equations for the LH_2 tank model are consistent with methodologies presented in [11,14], and only a high-level summary is provided for clarity/convenience. Figure 2 presents an overview of the cryogenic tank, illustrating the mass flow (black arrows) and heat flow (red arrows) paths.

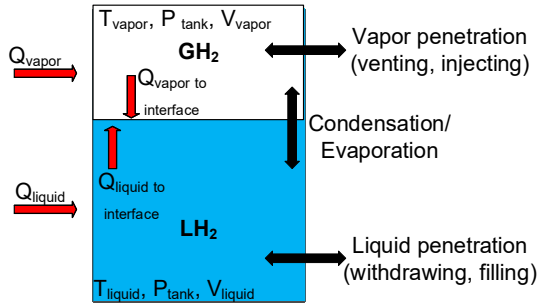


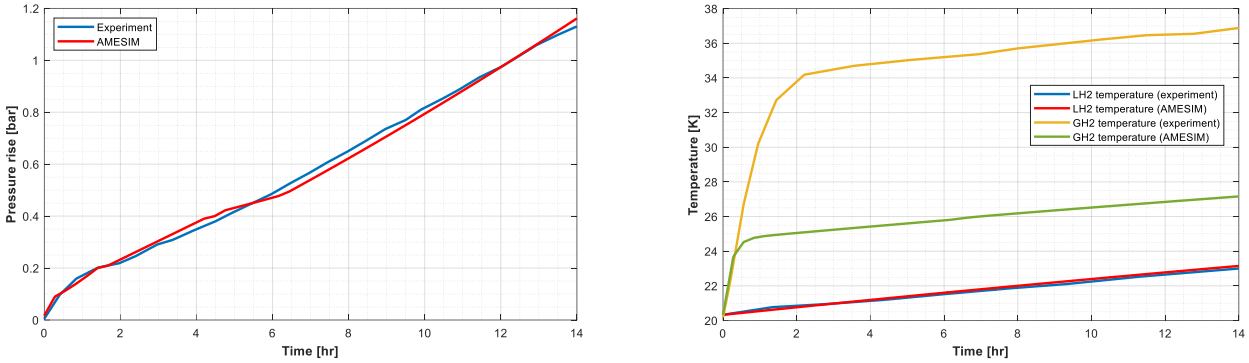
Figure 2. Mass flow and heat flow paths of a cryogenic tank.

The model validation was performed by benchmarking the Amesim simulation results against experimental results by Hasan et al. [15] (Figure 3). The tank had a roughly spherical shape with a diameter of 2.1 m and a volume of 4.89 m^3. It was filled with LH_2 at 83% of its total volume (the rest being gaseous hydrogen (GH_2)), maintained at a temperature of 20.33 K and a pressure of 1.03 bar. Additionally, the tank was subject to a constant heat flux of 3.5 W/m^2 for 14 h. In the model, hydrogen was treated as homogeneous ($v_g = v_l$, $P_g = P_l = P_{tank}$) and as parahydrogen. This assumption is valid since nearly 99.8% of hydrogen normally exists as parahydrogen at 20 K. Additionally, the conversion from para- to ortho-hydrogen on warming typically takes several hours [16]. Furthermore, the Helmholtz energy equation of state (EoS) was utilized during the simulation, as it provides the most accurate results across a wide validity domain [16]. The calculated pressure and temperature evolution for both the liquid and gaseous phases compared to available experimental data is shown in Figure 3a,b. Based on these data, the pressure rise curve matches the experimental data to within 5% after 14 h. Moreover, the temperatures of the liquid lines for both Amesim and the experiment are aligned perfectly. However, there is a significant difference (10 K) in gas temperatures, although the overall behavior remains the same. This discrepancy can be attributed to:

1. The real tank geometry was not completely spherical. In other words, it was the ellipsoidal volume that affected the height distribution as a function of volume.
2. The homogenous tank model does not account for temperature stratification. It assumes only two temperatures: one for the liquid phase and one for the gaseous phase, thereby neglecting the temperature profile expected in the vapor phase. As the distance from the liquid surface increases, the temperature of the gas should also increase. Because the temperature sensor was positioned in the upper region of the ullage, the measured vapor temperature in the experiment reflected the warm

region of the headspace. This value is expected to be higher than the average vapor temperature or the temperature near the liquid-vapor interface.

3. Amesim uses a simplified 0D modelling approach. Nevertheless, in the experiment, complicated physics in the 3D domain takes place.



(**a**) (**b**)

Figure 3. Cryogenic tank modelling validation for (**a**) pressure evolution and (**b**) temperature evolution over 14 h for the 3.5 W/m^2 case (Amesim vs. experiment [15]).

2.2. Simulation Scenarios Explanation

The baseline tank shape and its initial condition were comparable to those used for validation in Section 2.1 under stationary conditions. The tank was subject to a constant heat flow rate in the range of 0–500 W. The heat flow rate was distributed based on the wetted and dry surface areas as described in Equations (1)–(3).

$$Q = Q_v + Q_l \tag{1}$$

$$Q_l = Q \times A_w \tag{2}$$

$$Q_v = Q \times A_d = Q \times A\left(1 - \frac{A_w}{A}\right) \tag{3}$$

The wetted and dry surface areas of spherical and horizontal cylindrical tanks are defined in Table 1.

Table 1. Wetted and dry surface area expressions for spherical and horizontal cylindrical tanks.

Shape/Parameter	Spherical Tank	Horizontal Cylindrical Tank
Wetted area	$A_w = 2\pi Rh$	$A_w = 2RL\theta + \left(2R^2\theta - R^2\sin 2\theta\right)$
Dry area	$A_d = 4\pi R^2 - A_w$	$A_d = 2\pi RL + 2\pi R^2 - A_w$
Additional parameter	R= 1.05 m	$\theta = \arccos\left(\frac{R-h}{R}\right)$, $0 \le \theta \le \pi$, L= 1.4 m, R= 1.05 m

Where R, h, and L are the cross-sectional radius, the liquid height, and the cylinder length, respectively. The simulation scenarios are presented in Table 2.

Table 2. Simulation scenarios.

Scenario #	Description	Key Features/Conditions
1	LH_2 tank with constant heat flow rate without fuel withdrawal or pressure control system.	Closed system; only heat input considered.
2	Tank with constant heat flow rate and fuel withdrawal (from the tank) of 60 g/s, but no pressure control.	Heat input + steady fuel extraction; no active pressure regulation.

Table 2. *Cont.*

Scenario #	Description	Key Features/Conditions
3	Tank with constant heat flow rate, fuel withdrawal of 60 g/s, and pressure control system, but no venting.	Includes pressure regulation; venting excluded.
4	Tank with constant heat flow rate, fuel withdrawal rates of 60 g/s and 75 g/s, pressure control, and venting system.	Relief valve activates at 1.06 bar; variable LH_2 withdrawal rates.
5	Comparison of two tank geometries (spherical and horizontal cylindrical) with identical volume and diameter.	$V =$ 4.89 m^3, Diameter = 2.1 m; $q =$ 10–30 W/m^2, $\dot{m}_{extraction}$ = 60 g/s

3. Results

By replicating each scenario in the simulation platform, the following graphs (Figures 4–8) are illustrated. The simulation time for each scenario was set to 60 min.

Scenario #1: Constant heat flow rate, with no fuel withdrawal or pressure control.

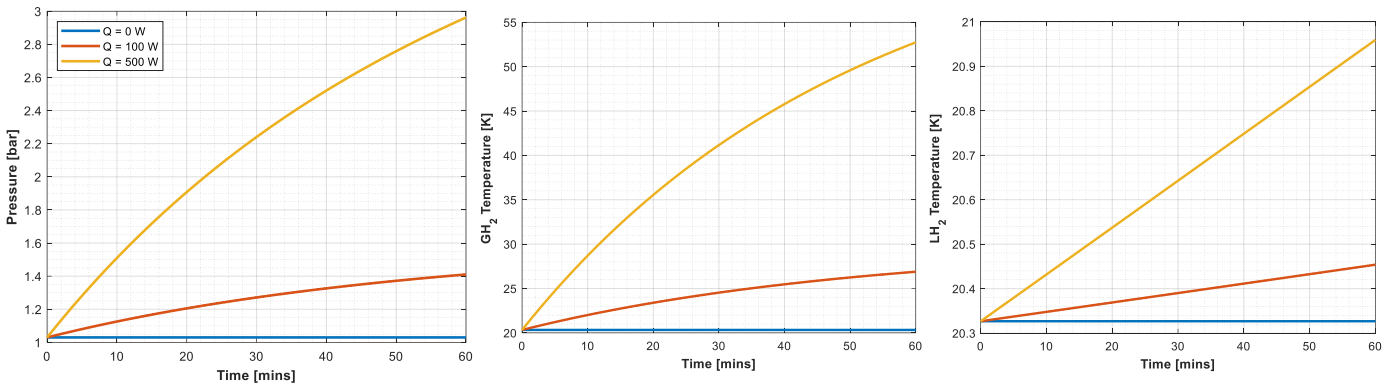


Figure 4. Time evolution for Scenario #1: (**a**) tank pressure, (**b**) GH_2 temperature, (**c**) LH_2 temperature.

Scenario #2: Constant heat flow, 60 g/s LH_2 withdrawal, and no pressure control.

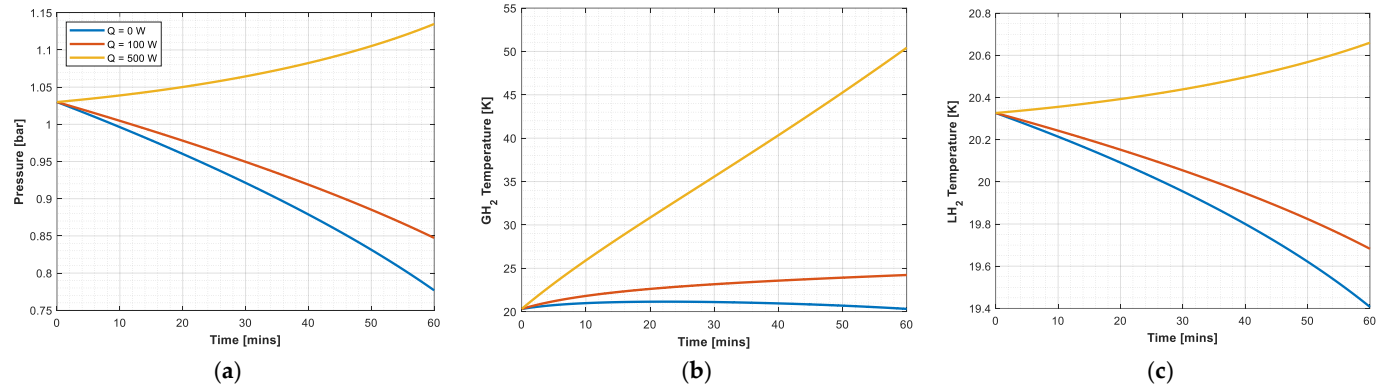


Figure 5. Time evolution for Scenario #2: (**a**) tank pressure, (**b**) GH_2 temperature, (**c**) LH_2 temperature.

Scenario #3: Constant heat flow, 60 g/s LH_2 withdrawal, pressure control.

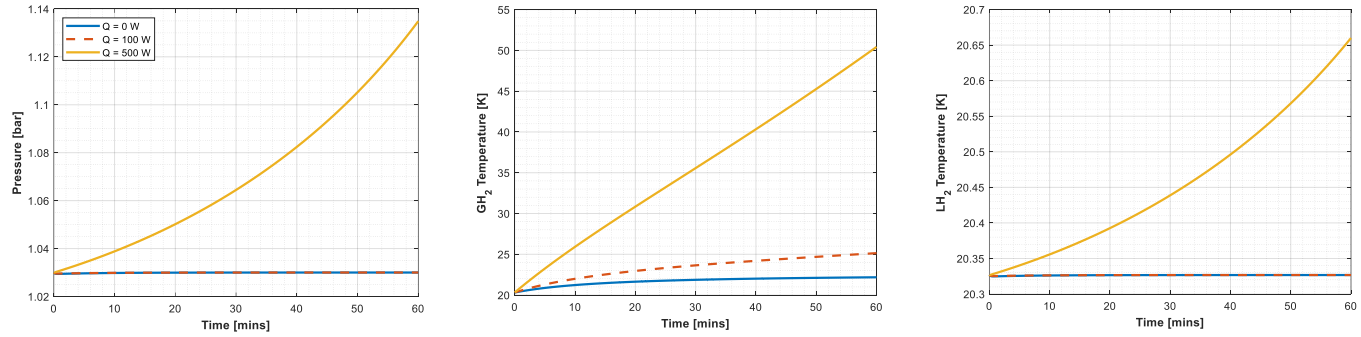


Figure 6. Time evolution for Scenario #3: (**a**) tank pressure, (**b**) GH_2 temperature, (**c**) LH_2 temperature.

Scenario #4: Constant heat flow, LH_2 withdrawal, pressure control and venting.

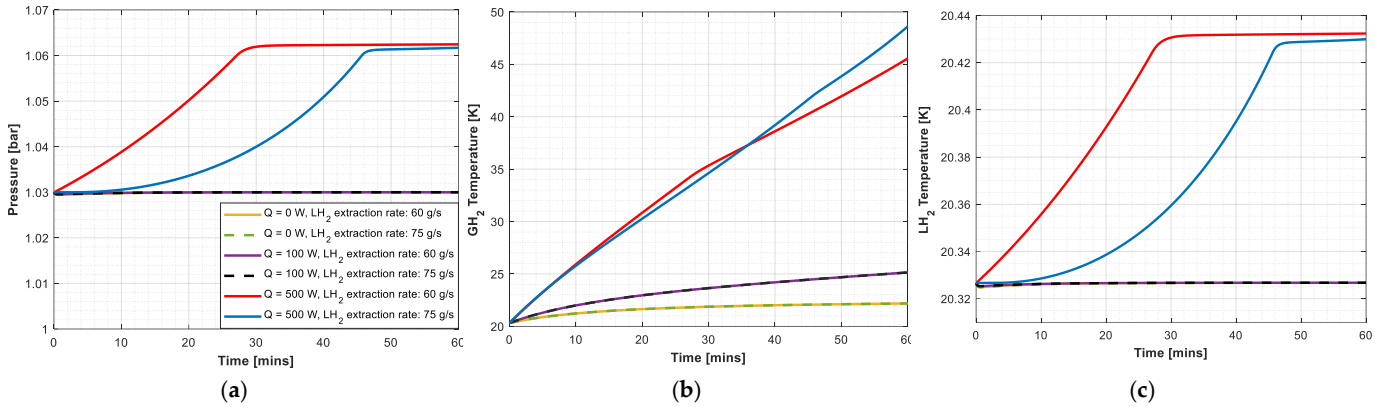


Figure 7. Time evolution for Scenario #4: (**a**) tank pressure, (**b**) GH_2 temperature, (**c**) LH_2 temperature.

Scenario #5: Comparison of tanks with different geometries.

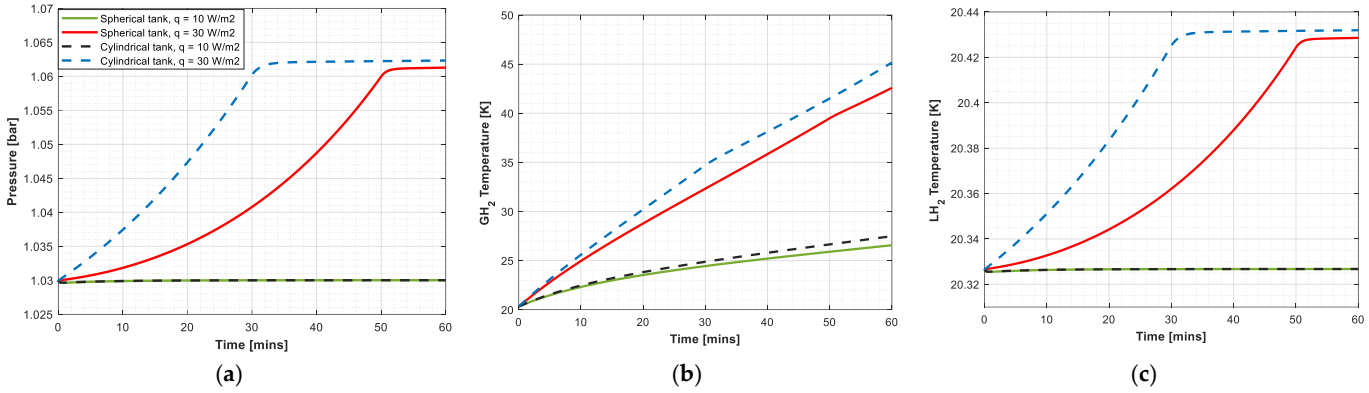


Figure 8. Spherical and horizontal cylindrical tank conditions over time for Scenario #5: (**a**) tank pressure, (**b**) GH_2 temperature, (**c**) LH_2 temperature.

4. Discussion

The observations based on the results presented in Section 3 are discussed as follows:

1. In Scenario #1, the tank pressure rose continuously over time, while the GH_2 temperature increased faster than the LH_2 temperature. Physically, this occurs because most of the heat entering through the upper dry wall warms the vapor first, raising its temperature and pressure. On the other hand, the liquid has a much higher thermal capacity and weak natural convection at cryogenic temperatures, so it warms much more slowly. Therefore, the bulk LH_2 temperature was below the saturation tempera-

ture corresponding to the measured pressure and hence, slightly subcooled (Figure 4). In this condition, the system was not at thermodynamic equilibrium.

2. In Scenario #2, the tank was considered an open system. The tank received the same heat input as Scenario #1, but LH_2 was continuously removed at 60 g/s. As LH_2 was withdrawn, the total liquid volume decreased, thereby increasing the vapor space volume in the tank. However, by increasing the total heat flow rate from 100 W to 500 W, the pressure drop caused by LH_2 extraction would be reduced. It is evident that at a 500 W heat flow rate, the tank pressure increased (Figure 5a), even with liquid fuel being withdrawn at 60 g/s. The LH_2 temperatures were in a saturated condition, as the tank was no longer a closed system.
3. In Scenario #3, a minimum pressure maintenance system was implemented by injecting regulated, superheated GH_2 to stabilize and maintain the tank pressure at the desired level of 1.03 bar. The system successfully maintained constant pressure (Figure 6a) for heat flow rates between 0 and 100 W. However, at a heat flow rate of 500 W, the thermal input exceeded the compensating effect of fuel withdrawal (see also Figure 5). Under these conditions, injecting additional superheated GH_2 from the minimum pressure maintenance system would have been unwanted and counterproductive. This demonstrates that a pressure control system relying solely on regulated GH_2 injection is insufficient to maintain the tank pressure within acceptable limits under high levels of heat ingress. The LH_2 temperatures were in a saturated state, similar to Scenario #3.
4. In Scenario #4, by introducing a venting system, the tank achieved a completely regulated pressure condition (Figure 7). For 0–100 W heat loads, the pressure and LH_2 temperature curves were identical for both 60 g/s and 75 g/s LH_2 withdrawal rates, as the effects of heat input and fuel removal compensated each other. For the 500 W heat load, increasing the mass withdrawal rate moderated the pressure increase behavior, acting as a cooling mechanism through convective and latent heat removal. For the GH_2 temperature, after some time, the GH_2 temperature in the 75 g/s case surpassed that of the 60 g/s case because the higher LH_2 withdrawal rate led to a smaller available liquid mass to absorb heat, resulting in more heat being retained in the vapor space, which pushed the GH_2 temperature higher. The LH_2 temperature followed the same trend as pressure, remaining in the saturated state.
5. In Scenario #5, under identical heat flux conditions, the spherical tank shows a slower increase in pressure and temperatures for both gaseous and liquid phases (Figure 8). This is due to the sphere's lower ratio of surface area to volume, which reduces heat ingress. For the low heat flux of 10 W/m^2, both the spherical and cylindrical tanks showed almost constant pressure of ~1.03 bar, indicating that the heat input was sufficiently low to be balanced by internal energy redistribution. The cylindrical tank, by contrast, received more heat per stored mass and developed stronger stratification in the vapor and liquid phases. In turn, this led to a steeper pressure rise, higher GH_2 temperature, and correspondingly faster LH_2 warming at the higher flux of 30 W/m^2 since LH_2 temperature closely followed the saturation temperature tied to pressure. Thus, the tank shape and the magnitude of the heat flux together significantly influence the transient pressurization and thermal behavior of cryogenic LH_2 storage systems. Tank orientation did not reveal first-order effects on the results.

5. Conclusions

This study addresses the critical need for a sensitivity analysis framework that links cryogenic thermodynamics, tank geometry, heat transfer behavior, LH_2 extraction, and pressurization control strategies in LH_2 storage systems. The paper presents five operational

scenarios: closed tank self-pressurization; open system LH_2 withdrawal; GH_2 injection from a minimum pressure maintenance system; vent-regulated LH_2 withdrawal, and geometry comparison under identical heat flux conditions, thereby providing a systematic basis for evaluating design trade-offs. The results from those scenarios show that: (1) Under completely passive self-pressurization, the tank pressure rises continuously and the GH_2 temperature increases much faster than the LH_2 because the liquid remains subcooled and not in thermodynamic equilibrium (Scenario #1). (2) The introduction of LH_2 extraction (open system) changes the heat mass balance. At high heat loads (500 W), the tank still pressurizes, but the LH_2 becomes saturated (Scenario #2). (3) A GH_2 injection-only minimum pressure control mechanism can maintain a set pressure only up to a moderate heat input. Beyond that heat input, the pressure rise is uncontrolled (Scenario #3). (4) By adding a venting mechanism, the tank pressure can be fully managed under variable LH_2 extraction. Moreover, higher LH_2 extraction can lead to higher GH_2 temperatures due to reduced liquid-phase buffering (Scenario #4). (5) Finally, the sensitivity study on geometry and heat flux demonstrates that spherical tanks respond more slowly (in terms of pressure and temperature rise) than horizontal cylindrical tanks. Further, at low heat fluxes (e.g., 10 W/m^2), both geometries maintain a nearly constant pressure (~1.03 bar), indicating that the heat leak is balanced by internal energy redistribution. At higher fluxes (e.g., 30 W/m^2), the geometry and surface-to-volume ratio dominate the transient behavior. Additionally, tank orientation had no first-order effects on the results (Scenario #5).

Author Contributions: Conceptualization, A.E. and A.R.; methodology, A.E.; software, A.E.; validation, A.E.; formal analysis, A.E., A.R., D.S. and B.D.J.S.; investigation, A.E.; writing—original draft preparation, A.E.; writing—review and editing, A.E., A.R. and B.D.J.S.; supervision, A.R., D.S. and B.D.J.S. All authors have read and agreed to the published version of the manuscript.

Funding: The work was supported by Innovate UK through funding the UK Aerospace Technology Institute (ATI) project: Future Engine Technology for the Control of Hydrogen (FETCH) under grant agreement No. 10065215.

Data Availability Statement: Data are contained within the article.

Acknowledgments: The authors thank the Moog aircraft group team (FETCH project lead) for their approval to present and publish this work under the FETCH project.

Conflicts of Interest: The authors declare no conflicts of interest.

References

1. IATA. *Hydrogen for Aviation—A Future Decarbonization Solution for Air Travel?* International Air Transport Association: Montreal, QC, Canada, 2025.
2. Job, S.; Campbell, M.; Hall, B.; Hamadache, Z.; Kumar, N. *Sustainability Report: The Lifecycle Impact of Hydrogen-Powered Aircraft*; FZO-STY-REP-0005; Aerospace Technology Institute—FlyZero: Beford, UK, 2022.
3. Ebrahimi, A.; Rolt, A.; Jafari, S.; Anton, J.H. A review on liquid hydrogen fuel systems in aircraft applications for gas turbine engines. *Int. J. Hydrogen Energy* **2024**, *91*, 88–105. [CrossRef]
4. Giannis, S.; Salmeron-Perez, N.; Spetsieris, N. *Challenges in Realising Composite Liquid Hydrogen Cryogenic Storage: A Materials and Standards Perspective*; National Physical Laboratory: Middlesex, UK, 2023. [CrossRef]
5. Aerospace Technology Institute, FlyZero. Available online: https://www.ati.org.uk/flyzero/ (accessed on 15 November 2022).
6. Airbus, ZEROe. Available online: https://www.airbus.com/en/innovation/energy-transition/hydrogen/zeroe-our-hydrogen-powered-aircraft (accessed on 1 November 2025).
7. Xisto, C.; Lundbladh, A. Design and Performance of Liquid Hydrogen Fuelled Aircraft for Year 2050 EIS. In Proceedings of the ICAS 2022 Congress, Stockholm, Sweden, 4–11 September 2022.
8. Huete, J.; Pilidis, P. Parametric Study on Tank Integration for Hydrogen Civil Aviation Propulsion Liquid Hydrogen MLI Multi-Layer Insulation VC Vacuum SAF Sustainable Aviation Fuel. *Int. J. Hydrogen Energy* **2021**, *46*, 37049–37062. [CrossRef]
9. Lvovich, V.F.; Johnson, W.L.; Vivod, S.L. Cryogenic Hydrogen Studies and Testing for Advanced Aircraft at NASA, 2025. Available online: https://ntrs.nasa.gov/citations/20250002550 (accessed on 5 November 2025).

10. Burschyk, T.; Fröhler, B.; Alder, M.; Zill, T. Global Sensitivity Analysis of Liquid Hydrogen Storage Design Parameters for Overall Aircraft Design. In Proceedings of the ICAS 2024 Congress, Florence, Italy, 9–13 September 2024.
11. Adler, E.J.; Martins, J.R.R.A. Liquid Hydrogen Tank Boil-off Model for Design and Optimization. *J. Thermophys. Heat Transf.* **2025**, *39*, T7005. [CrossRef]
12. Simcenter Amesim | Siemens Software. 2025. Available online: https://plm.sw.siemens.com/en-US/simcenter/systems-simulation/amesim/ (accessed on 1 November 2025).
13. Ebrahimi, A.; Sanders, D.; Rolt, A.; Sethi, V. Report on System Architecture Performance Analysis and Control, ZEST1 D1.4.3a.3, 2025.
14. Lin, C.-S.; Van Dresar, N.T.; Hasan, M.M. A Pressure Control Analysis of Cryogenic Storage Systems, 1991. Available online: https://ntrs.nasa.gov/citations/19910015147 (accessed on 10 October 2023).
15. Hasan, M.M.; Lin, C.S.; Van Dresar, N.T. Self-Pressurization of a Flightweight Liquid Hydrogen Storage Tank Subjected to Low Heat Flux. 1991. Available online: https://ntrs.nasa.gov/citations/19910011011 (accessed on 10 October 2023).
16. Leachman, J.; Jacobson, B.; Penoncello, S.; Lemmon, E. Fundamental Equations of State for Parahydrogen, Normal Hydrogen, and Orthohydrogen. *J. Phys. Chem. Ref. Data* **2009**, *38*, 721–748. [CrossRef]

Disclaimer/Publisher's Note: The statements, opinions and data contained in all publications are solely those of the individual author(s) and contributor(s) and not of MDPI and/or the editor(s). MDPI and/or the editor(s) disclaim responsibility for any injury to people or property resulting from any ideas, methods, instructions or products referred to in the content.